

Starting vortex dipoles in a viscous fluid: Asymptotic theory, numerical simulations, and laboratory experiments

Y. D. Afanasyev^{a)} and V. N. Korabel

Department of Physics and Physical Oceanography, Memorial University of Newfoundland, St. John's, Newfoundland A1B 3X7, Canada

(Received 21 January 2004; accepted 13 July 2004; published online 15 September 2004)

Translational velocity of the starting vortex dipoles generated by the continuous or impulsive action of a localized force is obtained theoretically on simple physical grounds. Solutions of the diffusion equation for vorticity which take into account the translational motion of fluid particles are then obtained and compared with the results of direct numerical simulations of vortex dipoles as well as with the laboratory experiments. The comparison shows good quantitative agreement in both cases. Theoretical results for the translational velocity of the three-dimensional (axisymmetric) flows such as starting jets or vortex rings are discussed as well. © 2004 American Institute of Physics.
[DOI: 10.1063/1.1790493]

I. INTRODUCTION

Organized dipolar vortex structures are a very well known feature of quasi-two-dimensional flows where motion in one direction is suppressed due to one of the following physical mechanisms: background rotation of the system, density stratification, or geometrical restrictions such as for the flows in thin layers or soap films. In an oceanographic context, vortex dipoles are often called mushroom-like currents since they resemble a sliced mushroom. Vortex dipoles are formed in a viscous fluid when a force is applied locally to some volume of fluid. If the force acts impulsively, a translating vortex dipole is generated. If the force starts at $t=0$ and then acts continuously, a starting jet with a dipole at its front is generated. Here we call the flow in both regimes starting vortex dipoles to emphasize the fact that the flow is unsteady. These flows have been previously studied theoretically and experimentally by many authors (e.g., Sozou,¹ Cantwell,² Afanasyev *et al.*,³ Voropayev *et al.*⁴). A review of the results as related to two-dimensional flows and flows in a stratified fluid is given by Voropayev and Afanasyev.⁵ Theoretical solutions were obtained for starting vortex dipoles in the Stokes approximation^{2,6} as well as in a weakly nonlinear approximation⁵ where the next term of the expansion in terms of a small parameter (the Reynolds number) was obtained. These solutions show good qualitative agreement with the experimental flows. In particular, the distributions of passive tracers in the flows can be easily obtained by integration of the velocity field obtained theoretically. These distributions demonstrate a typical mushroom-like pattern (Voropayev *et al.*⁴). The linear solutions in the Stokes approximation can also describe, in a qualitative manner, the flows generated by multiple forces if the appropriate superposition of the solutions is considered. The collisions of planar vortex dipoles were visualized using this method by Afanasyev *et al.*⁷ and compared with experimental results⁸ for

interactions of planar vortex dipoles in a stratified fluid. Although linear solutions reproduce the general features of the flows surprisingly well, they fail to describe the translational motion of the dipoles. The translational motion is due to advection and is therefore a nonlinear effect.

In the following sections of this paper we report on the results of the theoretical analysis of the starting dipoles, which allows us to take into account the translational motion of the dipoles (Sec. II). In our theoretical analysis we make a hypothesis regarding the velocity of the dipoles based on physical arguments and then test this hypothesis using a comparison of the theoretical solutions with the results of direct numerical simulations of the flows (Sec. III). This comparison demonstrates significant agreement which proves that the hypothesis is valid. The comparison of theory with our laboratory experiments is reported in Sec. IV. Conclusions as well as a discussion of the axisymmetric flows, such as starting jets in a density homogeneous fluid or planar (but three-dimensional) starting vortex dipoles in a continuously stratified fluid, are offered in Sec. V.

II. THEORY

Consider a two-dimensional planar flow in a viscous incompressible fluid induced by a localized forcing. The fluid extends to infinity and is initially at rest. A momentum source is located at the origin of the coordinate system. The momentum source starts acting at time $t=0$ and thereafter exerts on the fluid the kinematic momentum flux (force per unit mass and unit depth) equal to $J=\text{const}$. The dimensions of J are $[J]=L^3T^{-2}$, where L and T are the units of length and time. An impulsive source which acts for a short period of time delivering finite kinematic momentum $I([I]=L^3T^{-1})$ will be considered as well. The balance of momentum and the equation of continuity for a fluid with singularity at the origin can be presented in the form

$$\frac{\partial \mathbf{u}}{\partial t} + (\mathbf{u} \cdot \nabla) \mathbf{u} = -\frac{1}{\rho} \nabla p + \nu \nabla^2 \mathbf{u} + \mathbf{A} \delta(\mathbf{x}), \quad (1)$$

^{a)}Author to whom correspondence should be addressed; electronic mail: yakov@physics.mun.ca

$$\nabla \mathbf{u} = 0, \tag{2}$$

where u is the velocity vector, p is pressure, ν is the kinematic viscosity, $\mathbf{x}=(x,y)$ the position vector, and $\delta(\mathbf{x})$ is the Dirac delta function. The vector A represents the force of magnitude $JH(t)$ or $I\delta(t)$ applied in the positive direction along the x axis. Here $H(t)$ is the Heaviside step function.

The dimensionless amplitudes of forcing in the following form:

$$\text{Re}_J = \frac{Jt^{1/2}}{\nu^{3/2}}, \text{Re}_I = \frac{I}{\nu^{3/2}t^{1/2}},$$

have the physical meaning of the Reynolds number of the flow.^{2,5} Note, that there is no natural length scale in the problem since the momentum source is a point source.

A force acting at the origin generates dipolar vorticity in the vicinity of the origin. This vorticity is advected by the induced flow and diffuses. The far field of the flow is approximately irrotational (potential). The velocity in this region establishes instantaneously (in an incompressible fluid) according to the momentum equation at large $|x|$,

$$\frac{\partial \mathbf{u}}{\partial t} + \frac{1}{\rho} \nabla p = 0. \tag{3}$$

The pressure field can be found by taking the divergence of (1) and employing the fact that in two dimensions $2\pi\delta(\mathbf{x}) = -\nabla^2 \ln|\mathbf{x}|$. Taking into account the continuity equation (2) and neglecting the nonlinear terms, which are small at large $|x|$ (e.g., Cantwell²), one arrives at the Poisson equation

$$\nabla^2 \left(\frac{1}{\rho} p + \frac{A}{2\pi} \nabla \ln|\mathbf{x}| \right) = 0.$$

The particular solution of this equation is then

$$\frac{1}{\rho} p = \frac{\mathbf{A}\mathbf{n}}{2\pi|\mathbf{x}|} = |\mathbf{A}| \frac{\cos \theta}{2\pi r} = |\mathbf{A}| \frac{x}{2\pi(x^2 + y^2)}, \tag{4}$$

where $\mathbf{n}=\mathbf{x}/|\mathbf{x}|$ is the unit vector, and the polar coordinate system (r, θ) is used. As can be seen from (4), the pressure instantaneously arises in the fluid and does not change with time for the continuous source, while for the impulsive source there is a pressure impulse at $t=0$ and the pressure is zero at $t>0$.

The potential velocity distribution can then be obtained by integrating (3) with respect to time as follows:

$$\mathbf{u} = -Jt \frac{1}{2\pi} \nabla \left(\frac{x}{x^2 + y^2} \right) \text{ (continuous source),} \tag{5}$$

$$\mathbf{u} = -I \frac{1}{2\pi} \nabla \left(\frac{x}{x^2 + y^2} \right) \text{ (impulsive source).} \tag{6}$$

For small Reynolds numbers the momentum equation (1) can be linearized to obtain the equation in the Stokes approximation. The equation for vorticity in this approximation is of the form of the diffusion equation,

$$\frac{\partial \omega}{\partial t} = \nu \left(\frac{\partial^2 \omega}{\partial x^2} + \frac{\partial^2 \omega}{\partial y^2} \right). \tag{7}$$

This equation can be solved for different configurations of point forces (e.g., Cantwell,² Voropayev and Afanasyev⁵). The relation for pressure (4) can be used to relate the flow characteristics to the forcing amplitude (Voropayev *et al.*⁹). The particular solutions for the case of the impulsive source gives vorticity and stream function as follows:

$$\omega = \frac{Ir \sin \theta}{8\pi(\nu t)^2} e^{-r^2/4\nu t}, \tag{8}$$

$$\psi = \frac{I \sin \theta}{2\pi r} (1 - e^{-r^2/4\nu t}). \tag{9}$$

It was demonstrated⁵ that these solutions describe reasonably well the growth of the vortex dipole for small values of the Reynolds numbers. They fail, however, to describe the translational motion of the vortex dipole which is clearly due to the nonlinear effect of advection.

The linear solution is in fact a first-order term of the expansion of the full solution of the original equation (1) in terms of a small parameter, namely, the dimensionless forcing amplitude (Reynolds number). The linear solution can be improved if the next term in the expansion is added, thus rendering a weakly nonlinear solution. This second order term is quadratic in the Reynolds number and is proportional to $\sin 2\theta$ (Voropayev and Afanasyev⁵). The weakly nonlinear solution allows the vortex dipole to drift forward. This solution, however, does not correctly describe the velocity of propagation of the dipoles for moderate and large values of the Reynolds numbers.

Consider now the starting vortex dipoles generated either by a continuous or an impulsive forcing. We can derive the translational velocity of the dipoles using simple physical considerations. Consider a (Lagrangian) fluid particle located at the x axis just in front of the moving dipole. Linear solutions as well as direct numerical simulations demonstrate that vorticity is concentrated in the dipole and decays exponentially in front of the dipole (in the positive x direction). The flow in front of the dipole is therefore approximately irrotational and is described by (5) and (6). The distance traveled by the fluid particle can be obtained easily by integrating the x component of the potential velocity in (5) and (6) with respect to time to give

$$L(t) = \left(\frac{3J}{4\pi} \right)^{1/3} t^{2/3}, \tag{10}$$

$$L(t) = \left(\frac{3I}{2\pi} \right)^{1/3} t^{1/3} \tag{11}$$

for continuous and impulsive sources, respectively. The velocity of the propagation of the dipoles can then be introduced as $U=dL/dt$. The validity of the assumption that (10) and (11) describe the distance traveled by the dipoles can be investigated by comparing with the full solution of the equations of motion. Since such a solution is not available, we can do the next best thing by comparing with the results of

the direct numerical simulations for different values of the Reynolds number (appropriately nondimensionalized forcing parameter).

The vorticity created by the force at the origin translates according to (10) or (11) and diffuses. Since Eq. (7) is linear, the resulting vorticity field at any moment of time can be obtained by the integration of the previous distributions when the appropriate displacement of fluid particles and time delay are taken into account. The solution for the continuous source can then be easily obtained in the integral form,

$$\omega(x, y, t) = \frac{Jy}{8\pi\nu^2} \int_0^t \frac{1}{(t-\tau)^2} \exp\left[-\frac{[x-L(t-\tau)]^2 + y^2}{4\nu(t-\tau)}\right] d\tau, \tag{12}$$

$$\psi(x, y, t) = -\frac{Jy}{2\pi} \int_0^t \frac{1 - \exp\left[-\frac{[x-L(t-\tau)]^2 + y^2}{4\nu(t-\tau)}\right]}{[x-L(t-\tau)]^2 + y^2} d\tau, \tag{13}$$

where we substitute (10) for $L(t)$. The x and y velocity components can then be obtained by differentiation of (13) as follows:

$$u(x, y, t) = \frac{J}{\pi} \int_0^t \left[\frac{(1 - e^{-(x'^2+y^2)/4\nu\zeta})y^2}{(x'^2+y^2)^2} + \frac{(1 - e^{-(x'^2+y^2)/4\nu\zeta})}{2(x'^2+y^2)} + \frac{y^2 e^{-(x'^2+y^2)/4\nu\zeta}}{4\nu\zeta(x'^2+y^2)} \right] d\zeta, \tag{14}$$

$$v(x, y, t) = \frac{J}{\pi} \int_0^t \left[\frac{(1 - e^{-(x'^2+y^2)/4\nu\zeta})x'y}{(x'^2+y^2)^2} - \frac{x'y e^{-(x'^2+y^2)/4\nu\zeta}}{4\nu\zeta(x'^2+y^2)} \right] d\zeta. \tag{15}$$

Here we use the notation

$$x' = x - \left(\frac{3J}{4\pi}\right)^{1/3} \zeta^{2/3},$$

to make the expressions (14) and (15) more compact. Instantaneous streamlines calculated from (13), and the velocity field (14) and (15) demonstrate a typical pattern of the dipolar flow (Fig. 1).

The solution for the impulsive dipole can be obtained by performing a simple transformation of the x coordinate $x \rightarrow x-L(t)$ in the expressions (8) and (9) where $L(t)$ is given by (11). We do not need to integrate in this case because vorticity is only generated at $t=0$.

In the experiments, a passive tracer (usually a dye) is used to visualize the flow pattern. It is useful, therefore, to visualize the theoretical results in the same way. If the velocity components are known, it is possible to calculate the distributions of the marked particles at different times by integrating the equations of motion for marked particles such that

$$\frac{dx_p}{dt} = u(x, y, t), \quad \frac{dy_p}{dt} = v(x, y, t). \tag{16}$$

Such a system of ordinary differential equations, where the right-hand side is known, can be easily solved numerically

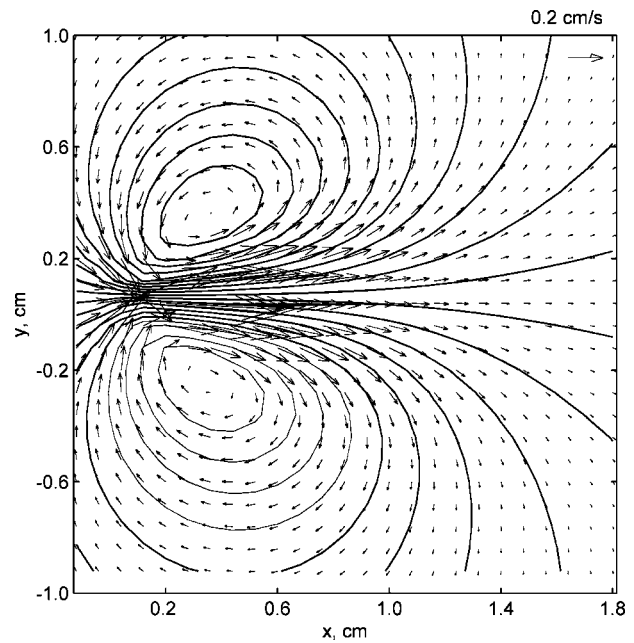


FIG. 1. Velocity field (arrows) and instantaneous stream function (contours) calculated from (13)–(15) for $J=0.05 \text{ cm}^3/\text{s}^2$ at $t=5 \text{ s}$.

using standard solvers available in various applied mathematical software packages. It is important, however, to specify initial conditions for the marked particles such that the calculations closely reproduce the experiments.

We performed a numerical integration of (16) for the case of the continuous dipole with the velocity components (14) and (15). In our calculations we launched 30 particles from a circle of radius $r=0.1 \text{ cm}$ with its center at the origin. The endpoints of the trajectories of all the injected particles at any time t gave the outline of the front of the dyed fluid (“hat of the mushroom”). The second series of particles was launched continuously at intervals of 0.1 s from one point at the circle. These particles gave the outline of the side surface of the dyed fluid (“leg of the mushroom”). A sequence of images in Fig. 2 shows that our theoretical solution generates a typical pattern of dyed fluid observed both in laboratory experiments and numerical simulations of vortex dipoles.

In the following section we perform the quantitative comparison of the theoretical results obtained for continuous and impulsive vortex dipoles with direct numerical simulations to show the validity of the hypothesis on the translational speed of the dipoles.

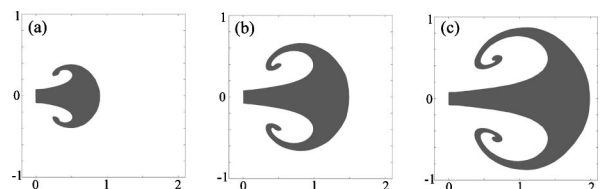


FIG. 2. A succession of images showing the distribution of marked particles in the continuous vortex dipole described by the velocity field (14) and (15). The values of control parameters in the model are: $\rho=1 \text{ g cm}^{-3}$, $\nu=0.01 \text{ cm}^2 \text{ s}^{-1}$, and $J=0.05 \text{ cm}^3 \text{ s}^{-2}$. Time $t=5 \text{ (a)}$, 10 (b) , 15 s (c) . Scale in cm.

TABLE I. Parameters of the numerical simulations.

| Simulations | J (cm ³ /s ²) | I (cm ³ /s ²) | a (cm) | n | aJ/ν^2 | $I/\nu\alpha$ | c |
|-------------|--|--|----------|------|------------|---------------|------|
| Continuous | | | | | | | |
| 1 | 0.05 | | 0.2 | 0.66 | 100 | | 0.23 |
| 2 | 0.126 | | 0.1 | 0.66 | 126 | | 0.37 |
| 3 | 0.50 | | 0.2 | 0.65 | 1000 | | 0.64 |
| 4 | 1.0 | | 0.2 | 0.67 | 2000 | | 1.1 |
| 5 | 3.15 | | 0.5 | 0.68 | 15 700 | | 2.7 |
| Impulsive | | | | | | | |
| 6 | | 0.63 | 0.1 | ... | | 630 | ... |
| 7 | | 15.75 | 0.5 | 0.35 | | 3140 | 2.6 |
| 8 | | 12.6 | 0.2 | 0.34 | | 6300 | 2.2 |
| 9 | | 18.8 | 0.2 | 0.34 | | 9400 | 3.1 |

III. COMPARISON WITH THE NUMERICAL SIMULATIONS

A series of two-dimensional numerical simulations that document the dipolar flow generated by a localized forcing has been performed using commercial computational fluid dynamics code FLUENT 6.0.2 on the SGI Onyx 3400 computer. Finite element method simulations were carried out using a Navier–Stokes solver. The computational domain of dimensions 60 cm × 30 cm was used in our simulations and no-slip boundary conditions were applied at the walls to model the experiments in a laboratory tank. The domain was large enough to neglect the effect of the walls on the flow during the entire period of the flow evolution (10–50 s). The domain was filled with an unstructured grid consisting of 85 000 triangular elements with a minimum mesh size of 0.027 cm. The size of the elements was smaller near the origin where the momentum source was located. The working fluid was water of density $\rho=0.998$ g/cm³ and kinematic viscosity $\nu=0.01$ cm²/s. A localized force ρJ was applied to a fluid in a circle of radius $a=0.1–0.5$ cm such that the force density f (force per unit area) is described by the Gaussian distribution $f=f_0 \exp(-r^2/a^2)$. The amplitude of the force f^0 and the radius of the circle a were varied in our simulations.

To analyze the results of the numerical simulations, it is useful to perform simple dimensional analysis of the control parameters involved in the problem. Consider the distance L traveled by a dipole measured from the origin to the centers of the vortices of the dipole measured along the x axis. L depends on the set of four dimensional quantities including kinematic viscosity ν , time t , the amplitude of forcing J (or I for the impulsive dipoles), and the size of the region where the force is applied, a . Dimensional analysis then gives

$$L = \left(\frac{3J}{4\pi}\right)^{1/3} t^{2/3} \Phi\left(\frac{Jt^{1/2}}{\nu^{3/2}}, \frac{Ja}{\nu^2}\right), \tag{17}$$

$$L = \left(\frac{3I}{2\pi}\right)^{1/3} t^{1/3} \Phi\left(\frac{I}{\nu^{3/2}t^{1/2}}, \frac{I}{\alpha\nu}\right), \tag{18}$$

where the numerical coefficients have been introduced to match these expressions with those for potential flow (10) and (11). Φ is an unknown function of two dimensionless arguments. The first argument, $\Pi_1=(Jt^{1/2})/\nu^{3/2}$ [$\Pi_1=I/(\nu^{3/2}t^{1/2})$], of the function Φ includes viscosity and is effectively the Reynolds number of the flow. It is time dependent and grows with time for continuous dipoles and decreases for impulsive dipoles. The second argument, $\Pi_2=(Ja)/\nu^2$ [$\Pi_2=I/(\alpha\nu)$], includes a and represents the effect of the finite size of the source.

Several simulations with different values of the amplitude of forcing and the size of the source were performed for continuous and impulsive sources. The main control parameters of the simulations are summarized in Table I. Measurements of the distance traveled by the dipoles (Figs. 3 and 4) demonstrate that the asymptotic regime of the flows is characterized by the time dependences, $L \sim t^{2/3}$ for continuous dipoles and $L \sim t^{1/3}$ for impulsive dipoles, in accord with those predicted by (10) and (11). Measured exponents for the numerically simulated flows are $n=0.66 \pm 0.01$ (continuous) and $n=0.34 \pm 0.01$ (impulsive). These results allow us to

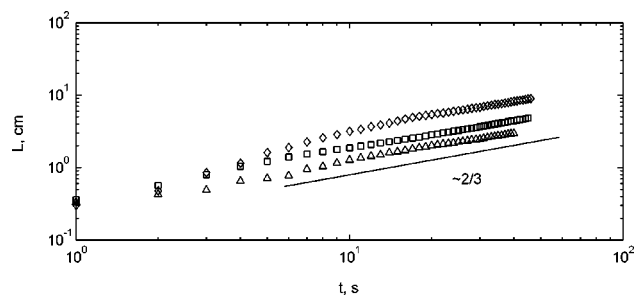


FIG. 3. Distance L for continuous dipoles for simulations 1 (triangles), 2 (squares), and 3 (diamonds) in Table I.

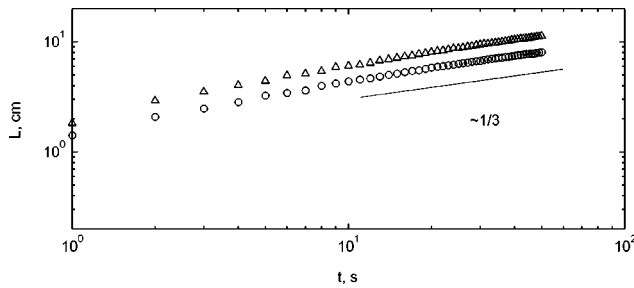


FIG. 4. Distance L for impulsive dipoles for simulations 7 (triangles) and 8 (circles) in Table I.

make a conclusion about the asymptotic behavior of the function Φ in (17) and (18) for large values of its first argument. To satisfy the results of the measurements, this function must not depend on time. Therefore, we can assume complete similarity of this function with respect to Π_1 ,

$$\Phi\left(\frac{Jt^{1/2}}{\nu^{3/2}} \rightarrow \infty, \frac{Ja}{\nu^2}\right) = G\left(\frac{Ja}{\nu^2}\right),$$

$$\Phi\left(\frac{I}{\nu^{3/2}t^{1/2}} \rightarrow \infty, \frac{I}{a\nu}\right) = G\left(\frac{I}{a\nu}\right).$$

For impulsive dipoles, Π_1 decreases with time and the asymptotic regime can be expected to exist only for intermediate times when Π_1 is still large. At large times, a viscous regime should be established in this case. The translational velocity of the dipole at the viscous regime should be described by the asymptotic expression $U=I/(32\pi\nu t)$ obtained by Cantwell and Rott.¹⁰ The decay in this regime is faster than that described by (11).

The values of the coefficient c in the dependence $L = ct^{2/3}$ ($L=ct^{1/3}$) were then measured and compared with the theoretically predicted values of the coefficient $c_t = (3J/4\pi)^{1/3}$ ($c_t=(3I/2\pi)^{1/3}$). The graph in Fig. 5 for continuous dipoles demonstrates that the measured coefficient approaches the theoretical value for the simulations where the parameter $\Pi_2=(Ja)/\nu^2$ is relatively small. This corresponds to a more concentrated (smaller a) and weaker source (smaller J). The asymptotic behavior of the function G ,

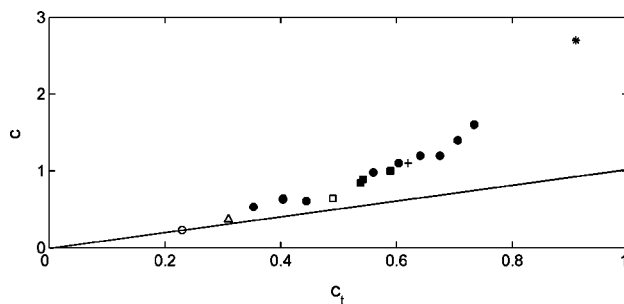


FIG. 5. Coefficient c measured in the numerical simulations and laboratory experiments vs the theoretical values of the coefficient. Simulations are shown by different symbols for different values of parameter Π_2 : 1 (circle), 2 (triangle), 3 (square), 4 (plus), and 5 (star). Experiments 1–10 in Table II are shown by filled circles. Experiments 11–13 are shown by filled squares. Solid line is $c=c_t$.

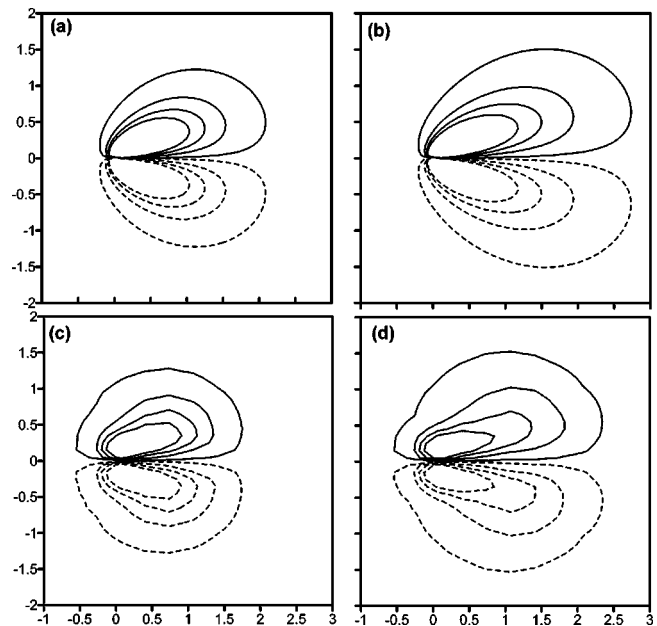


FIG. 6. Vorticity contours for a continuous vortex dipole: (a), (b) calculated from the theoretical relation (12) and (c), (d) are obtained in numerical simulation 1 (Table I). Contours are from -0.65 to 0.65 with the interval 0.2 s^{-1} . Streak lines are negative vorticity contours. $J=0.05 \text{ cm}^3/\text{s}^2$, $t=15 \text{ s}$ (a), (c) and $t=25 \text{ s}$ (b), (d). Scale in cm.

therefore, can be characterized as a complete similarity of this function with respect to its argument for small values of the argument

$$G\left(\frac{Ja}{\nu^2} \rightarrow 0\right) \rightarrow 1.$$

The values of the coefficient c for impulsive dipoles are given in Table I. They indicate similar properties of the function G with respect to $\Pi_2=I/(a\nu)$. Surprisingly this also indicates that this asymptotic behavior is achieved for larger values of a in contrast to the case of continuous dipoles where a must be small in order for Π_2 to be small. In simulation 6 (Table I) where the forcing was very weak, the intermediate asymptotic behavior was not observed. Since the initial Reynolds number of the flow was small the flow was in a viscous regime where no significant translation of the dipole was observed after a time interval of a few seconds.

Our numerical simulations demonstrate that global characteristics of the dipole, such as the distance L , is predicted well by theory. It is also interesting to compare the entire vorticity fields for the numerically simulated dipoles with those given by theory (12). Figure 6 shows a good quantitative agreement between the simulated dipole and theory. To find out if our theory indeed provides us with improved solution for moderate Reynolds numbers it is also useful to compare it with a weakly nonlinear solution obtained previously.⁵ The weakly nonlinear solution is given by the sum of dipolar and quadrupolar terms as follows:

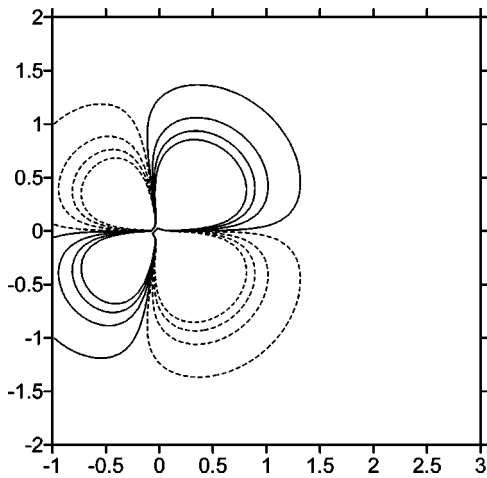


FIG. 7. Vorticity contours for a continuous vortex dipole calculated from the theoretical relation (19). Contours are from -0.65 to 0.65 with the interval 0.2 s^{-1} . $J=0.05 \text{ cm}^3/\text{s}^2$ and $t=15 \text{ s}$. Scale in cm.

$$\omega = \text{Re} \frac{\nu}{r^2} [W_1(\eta) \sin \theta + \text{Re} W_2(\eta) \sin 2\theta]. \quad (19)$$

Here $\text{Re}=Jr/(2\pi\nu^2)$ and $\eta=r/(2\sqrt{\nu t})$. Expressions for W_1 and W_2 are given in Voropayev and Afanasyev⁵ (they are not reproduced here because the expression for W_2 is quite lengthy). Solution (19) is valid for $\text{Re} \ll 1$. For the particular value of $J=0.05 \text{ cm}^3/\text{s}^2$ used for the flow demonstrated in Fig. 6, the solution (19) is only valid in a very small area near the origin where $r \ll 0.01 \text{ cm}$. At $t=15 \text{ s}$ [Figs. 6(a) and 6(c)], however, the vortical flow occupies already a much larger region. The pattern of vorticity contours (Fig. 7) for solution (19) reveals that the quadrupolar term prevails and that this solution does not provide accurate description of the flow (except near the origin). Thus, the weakly nonlinear solution (19) can only be used either for smaller J or smaller r (or equivalently smaller t) compared to the new solution (12) presented herein.

Solution (12) is obtained for the flow induced by the point forcing and its application is limited when the flows are generated by the distributed forcing. Figure 8 demonstrates

the comparison between the flow given by theory (18) and the numerically simulated flow for the simulation with higher Π_2 . Differences in the pattern of the vorticity distribution can be clearly seen in Fig. 8. There is a developed dipole in the frontal part of the starting flow in the numerical simulations. This dipole detaches somewhat from the jet flow which establishes behind it and moves faster than it should according to theory. This can also be seen from the fact that the difference between the coefficient c in simulations and in theory increases for larger values of the parameter Π_2 . Note that the predicted exponent in the time dependence $L \sim t^{2/3}$ is still valid for large Π_2 .

IV. COMPARISON WITH LABORATORY EXPERIMENTS

The laboratory experiments reported herein were performed using two different methods of forcing. In the first series of experiments an electromagnetic method of forcing was employed in a system of two thin layers of different density. Two layers were used to minimize the vertical component of velocity, providing the two dimensionality of the flow (e.g., Paret *et al.*¹¹). The particular parameters of our system were the same as those used in our previous experiments with two-dimensional turbulence (Wells and Afanasyev¹²). This system was shown to work well in achieving this purpose. In particular, an important result of that study was the growth of the Reynolds number of the flow which was in agreement with the predictions for the two-dimensional (2D) turbulence (e.g., Chasnov¹³). This growth was previously achieved only for the flows in soap films (Martin *et al.*¹⁴). This provides additional evidence of the 2D dynamics of the flow. In a thin layer system bottom friction is an important factor which prevents the flow from being purely two dimensional. Bottom friction as well as friction due to ordinary viscosity causes the total energy of the flow to decay (e.g., Danilov *et al.*¹⁵). It is important therefore to keep the rate of energy decrease due to bottom friction to be somewhat less than that due to ordinary viscosity. It was demonstrated to be the case in Wells and Afanasyev.¹² We assume that this is also true for the present experiments where the magnitude of forcing is similar to that

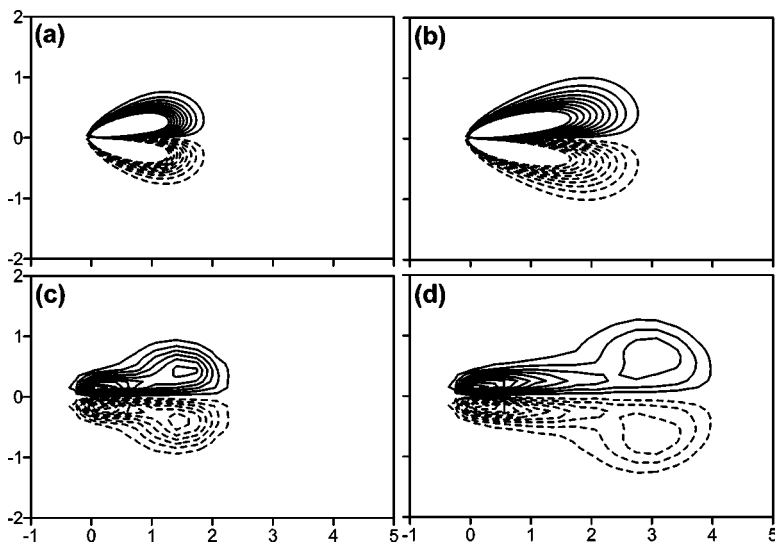


FIG. 8. Vorticity contours for continuous vortex dipole: (a), (b) calculated from the theoretical relation (12) and (c), (d) are obtained in numerical simulation 3 (Table I). Contours are from -5 to 5 with the interval 1 s^{-1} . $J=0.5 \text{ cm}^3/\text{s}^2$, $t=5 \text{ s}$ (a), (c) and $t=10 \text{ s}$ (b), (d). Scale in cm.

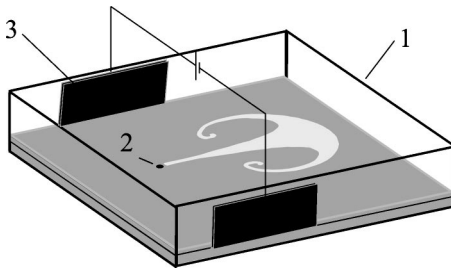


FIG. 9. Sketch of the experimental setup: tank (1), electrodes (2), and magnet (3).

used previously. The experiments were carried out in a rectangular container (Fig. 9) of inner dimensions $L=29$ cm and $W=21$ cm. The container was filled with two layers of salt water of depth 0.5 cm each and of concentration 40 and 250 g/l. The flow was forced electromagnetically by imposing an electric current of magnitude $j=0-3$ A in the horizontal direction. A rare earth permanent magnet of diameter 0.5 cm was placed flush with the bottom of the container. The magnet produces a magnetic field with a vertical component of ≈ 0.09 T. The interaction of the magnetic field with the electric current results in a horizontal force exerted locally on the fluid in the direction perpendicular to the electric current. This localized force generates a vortex dipole (Fig. 10) and the magnitude of the force can be controlled by varying the current. Parameters of the experiments are summarized in Table II (experiments 1–10). The flow was visualized by pH-indicator thymol blue and recorded using a digital video camera placed above the container. Geometrical characteristics of the flow were then measured using the in-

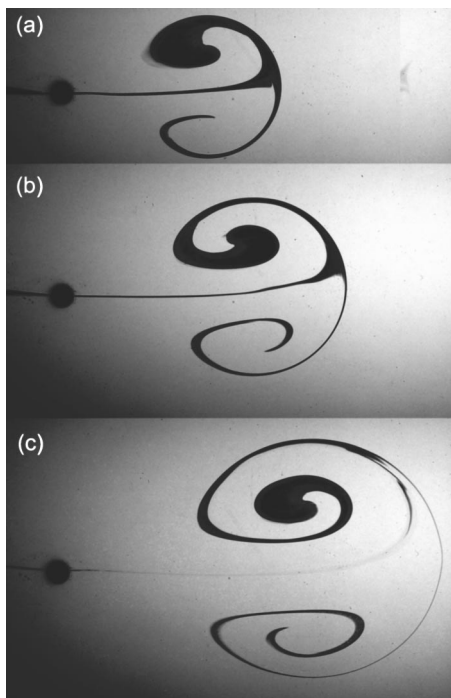


FIG. 10. Typical view of the developing continuous vortex dipole in the laboratory experiment. Current 0.3 A, $t=15$ s (a), 18 s (b), and 30 s (c). Black circle is the magnet of diameter 0.5 cm.

TABLE II. Experimental parameters.

| Experiment | Current (A) | J (cm ³ /s ²) | n | c |
|------------|-------------|--|------|------|
| 1 | 0.2 | | 0.67 | 0.53 |
| 2 | 0.3 | | 0.66 | 0.63 |
| 3 | 0.3 | | 0.62 | 0.64 |
| 4 | 0.4 | | 0.63 | 0.61 |
| 5 | 0.8 | | 0.60 | 0.98 |
| 6 | 1 | | 0.65 | 1.1 |
| 7 | 1.2 | | 0.61 | 1.2 |
| 8 | 1.4 | | 0.63 | 1.2 |
| 9 | 1.6 | | 0.67 | 1.4 |
| 10 | 1.8 | | 0.69 | 1.6 |
| 11 | | 0.65 | 0.66 | 1 |
| 12 | | 0.67 | 0.73 | 0.89 |
| 13 | | 0.86 | 0.72 | 0.84 |

dividual frames of a video sequence. The horizontal velocity field in the flow was measured using a PIV technique. A description of the method and general technique is given by Fincham and Spedding¹⁶ and Pawlak and Armi.¹⁷ The seeding particles were polyamid spheres of mean diameter 50 μm which were made visible by illuminating the fluid with a sheet of light at the interface between the layers. Top images of the flow are taken with a digital video camera. The video sequences have been processed to obtain the velocity fields. The profiles of the x component of the velocity across the jet region of the dipole, where the flow is established after the frontal part of the flow has passed, were integrated to obtain the values of momentum flux in the jet. The values of the flux were approximately equal for different sections of the jet along the x axis which confirms the fact that the flow is steady in this region. The momentum flux is generated by the electromagnetic forcing. These measurements, therefore, allow us to obtain the values of the control parameter J for different values of electric current in the tank. The linear relation was found of the form $J=0.92j$ where J is in cm³/s² and j is in A. Here we assumed that the flow is approximately uniform in the vertical direction along the depth of the layer (except in the thin boundary layer at the bottom).

In the second series of experiments the flow was forced using the injection of fluid through a nozzle in the form of a thin vertical slit of width $d=0.013$ cm and height $h=1$ cm. The layer of depth 1 cm was a solution of pH-indicator thymol blue of homogeneous density. In these experiments the momentum flux generated by the source can be measured directly by measuring the volume flux q through the nozzle. The momentum flux per unit depth of the layer can then be estimated as follows:

$$J = \frac{q^2}{dh}.$$

This method, though it provides a convenient method of measuring the main control parameter of the flow, is somewhat more challenging than that used in the experiments in a two-layer fluid as it is more difficult to avoid disturbances due to small density differences between the dyed fluid in-

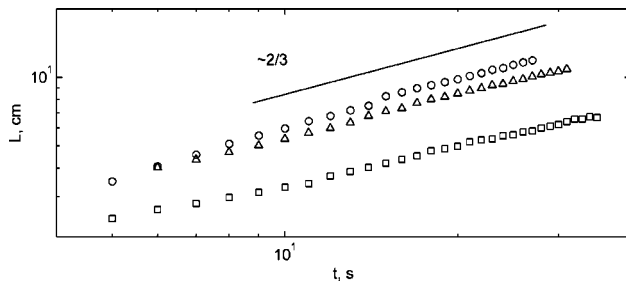


FIG. 11. Distance L for different times measured for continuous dipoles in the laboratory experiments 1 (squares), 3 (triangles), and 5 (circles) in Table II.

jected from the nozzle and the fluid in the tank. To avoid this problem we used the pH indicator for the visualization of the flows rather than regular dyes. However, these experiments were conducted only for the limited range of the variation of the momentum flux J . Parameters of the experiments are summarized in Table II (experiments 11–13).

Measurements of the distance L traveled by the dipoles in both series of the experiments (Fig. 11) gave results that were similar to those obtained in the numerical simulations. The measured exponent for the laboratory flows was $n = 0.66 \pm 0.04$ (Table II) for the asymptotic regime of the flow evolution. The values of the coefficient c are given in Table II and plotted in Fig. 5 together with the similar data from the numerical simulations. The graph shows that laboratory experiments are in accordance with the numerical simulations. The same tendency for the measured coefficients to deflect from their theoretical values with larger J is observed. This is the result of the finite extent of the forcing region which is approximately equal to the size of the magnet $2a = 0.5$ cm in the experiments.

V. DISCUSSION AND CONCLUDING REMARKS

In summary, it can be concluded that the theoretical analysis reported in this article provides an accurate approximation of the flow for continuous and impulsive starting dipoles. Our hypothesis on the velocity of the stream which is required for this approximation turned out to be quite accurate as demonstrated by the quantitative comparison of the theoretical results with the results of our numerical simulations of dipoles as well as with the results of laboratory experiments. The theoretical result which predicts the power law asymptotic behavior of the flow turned out to be especially robust even when additional factors such as the bottom friction in the laboratory experiments affect the flow.

The analysis of translational motion of the vortex structure at the front of a starting jet, similar to that developed in this paper for planar flows, can easily be performed for axisymmetric flows in a homogeneous fluid. The theory for the axisymmetric wake is reported by Afanasyev.¹⁸ Here, we would only like to discuss the speed of translational motion of the vortex structures. If a force acts for a short period of time in a homogeneous fluid, vortex rings are generated (e.g., Figs. 7.2.2 and 7.2.3 by Batchelor¹⁹). If the force acts continuously, a starting jet with a toroidal (mushroom-like) vortex at its front is generated (e.g., Fig. 1 by Voropayev²⁰).

From the expression for pressure similar to (4) (e.g., Voropayev *et al.*⁹) one can obtain the x component of the potential velocity:

$$u = -Jt \frac{1}{4\pi} \frac{\partial}{\partial x} \left(\frac{x}{|\mathbf{x}|^3} \right) \text{ (continuous source),} \tag{20}$$

$$u = -I \frac{1}{4\pi} \frac{\partial}{\partial x} \left(\frac{x}{|\mathbf{x}|^3} \right) \text{ (impulsive source).} \tag{21}$$

Note that the dimensions of the force amplitudes $[J] = L^4 T^{-2}$ and $[I] = L^4 T^{-1}$ are different from those in the planar case. The displacement of the starting axisymmetric vortices for continuous and impulsive sources, respectively, can then be obtained similar to (10) and (11) in the form

$$L(t) = \left(\frac{J}{\pi} \right)^{1/4} t^{1/2}, \tag{22}$$

$$L(t) = \left(\frac{2I}{\pi} \right)^{1/4} t^{1/4}. \tag{23}$$

This result allows us to explain the experimental results¹⁹ where the dependence $L \sim t^{1/2}$ was observed for a starting axisymmetric flow in a density homogeneous fluid. It is interesting to note that the same dependence was also observed in the experiments where starting dipoles were generated in a continuously (linearly) stratified fluid.^{3,4} The dipoles were generated by a continuous source acting in the horizontal direction. The effect of stratification was therefore to make the flows planar. The flows were planar because the vertical velocity was effectively suppressed. They were not, however, two dimensional since the flow expanded in the vertical direction due to viscous diffusion of the momentum. The indication of this intrinsic three dimensionality was the behavior of the global characteristic of the flow such as the length of the dipole L which varied in accordance with the dependence $L \sim t^{1/2}$, as predicted by (22) for three-dimensional flows.

The results obtained herein allow us to offer a simple test for two dimensionality of a liquid system in laboratory experiments. This is important in the experiments where it is desirable to achieve a flow which is as close as possible to being two dimensional such as, for example, in the experiments with two-dimensional turbulence. A continuous dipole can be generated in such a system by a forcing of the magnitude characteristic for the particular experiment planned in this system. If the dipole exhibits the asymptotic regime where $L \sim t^{2/3}$, the system is close to two dimensional. If, on the other hand, $L \sim t^{1/2}$ the system is rather three dimensional.

ACKNOWLEDGMENTS

The research reported in this paper has been supported by the Natural Sciences and Engineering Research Council of Canada under Grant Nos. 228941-2000 and 227192-2000.

¹C. Sozou, "Development of the flow field of a point force in an infinite fluid," *J. Fluid Mech.* **91**, 541 (1979).

²B. J. Cantwell, "Viscous starting jets," *J. Fluid Mech.* **173**, 159 (1986).

³Y. D. Afanasyev, S. I. Voropayev, and I. A. Filippov, "A model of the

- mushroom-like currents in a stratified fluid when a source of momentum acts continuously," *Izv., Acad. Sci., USSR, Atmos. Oceanic Phys.* **25**, 741 (1989).
- ⁴S. I. Voropayev, Y. D. Afanasyev, and I. A. Filippov, "Horizontal jets and vortex dipoles in a stratified fluid," *J. Fluid Mech.* **227**, 543 (1991).
- ⁵S. I. Voropayev and Y. D. Afanasyev, *Vortex Structures in a Stratified Fluid* (Chapman and Hall, London, 1994).
- ⁶Y. D. Afanasyev and S. I. Voropayev, "On the spiral structure of the mushroom-like currents in the ocean," *Dokl. Akad. Nauk USSR* **42**, 179 (1989).
- ⁷Y. D. Afanasyev, S. I. Voropayev, and P. G. Potylitsin, "A model of vortex dipole interactions in the upper ocean," *Atmos. Oceanic Phys.* **30**, 696 (1993).
- ⁸S. I. Voropayev and Y. D. Afanasyev, "Two-dimensional vortex dipoles interactions in a stratified fluid," *J. Fluid Mech.* **236**, 665 (1992).
- ⁹S. I. Voropayev, Y. D. Afanasyev, V. N. Korabel, and I. A. Filippov, "On the frontal collision of two round jets in water," *Phys. Fluids* **15**, 3429 (2003).
- ¹⁰B. Cantwell and N. Rott, "The decay of a viscous vortex pair," *Phys. Fluids* **31**, 3213 (1988).
- ¹¹J. Paret, D. Marteau, O. Paireau, and P. Tabeling, "Are flows electromagnetically forced in thin stratified layers two dimensional," *Phys. Fluids* **9**, 3102 (1997).
- ¹²J. Wells and Y. D. Afanasyev, "Decaying quasi-two-dimensional turbulence in a rectangular container: laboratory experiments," *Geophys. Astrophys. Fluid Dyn.* **98**, 1 (2004).
- ¹³J. R. Chasnov, "On the decay of two-dimensional homogeneous turbulence," *Phys. Fluids* **9**, 171 (1997).
- ¹⁴B. K. Martin, X. L. Wu, W. I. Goldburg, and M. A. Rutgers, "Spectra of decaying turbulence in a soap film," *Phys. Rev. Lett.* **80**, 3964 (1998).
- ¹⁵S. Danilov, F. V. Dolzhanskii, V. A. Dovzhenko, and V. A. Krymov, "Experiments on free decay of quasi-two-dimensional turbulent flows," *Phys. Rev. E* **65**, 036316 (2002).
- ¹⁶A. Fincham and G. Spedding, "Low cost, high resolution DPIV for measurement of turbulent fluid flow," *Exp. Fluids* **23**, 449 (1997).
- ¹⁷G. Pawlak and L. Armi, "Vortex dynamics in a spatially accelerating shear layer," *J. Fluid Mech.* **376**, 1 (1998).
- ¹⁸Y. D. Afanasyev, "Wakes behind towed and self-propelled bodies: Asymptotic theory," *Phys. Fluids* **16**, 3235 (2004).
- ¹⁹G. K. Batchelor, *An Introduction to Fluid Dynamics* (Cambridge University Press, Cambridge, 1967).
- ²⁰S. I. Voropayev, "Theory of the self-similar development of a jet in a uniform-density fluid," *Izv., Acad. Sci., USSR, Atmos. Oceanic Phys.* **21**, 975 (1985).